

THE CRYSTALLIZATION OF POTASSIUM GERMANATE GLASS WITH HIGH CONTENT OF NIOBIUM OXIDE

SRĐAN D.MATIJAŠEVIĆ,[#]MIHAJLO B.TOŠIĆ, JOVICA N. STOJANOVIĆ, SNEŽANA R.GRUJIĆ*, VLADIMIR D.ŽIVANOVIĆ, JELENA D.NIKOLIĆ, MARIJA S.ĐOŠIĆ

*Institute for Technology of Nuclear and Other Mineral Raw Materials,
86 Franchet d'Esperey St., 11000 Belgrade, Serbia*

**Faculty of Technology and Metallurgy, University of Belgrade,
4 Karnegijeva St., 11000 Belgrade, Serbia*

#E-mail: m.tosic@itnms.ac.rs

Submitted July 11, 2011; accepted November 4, 2011

Keywords: Germanate glass, Niobium oxide, Crystallization

Potassium germanate glass with molar ratio $[GeO_2]/[K_2O] = 1.2$ and Nb_2O_5 content of 34 mol% have been synthesized by a melt-quenching method. The crystallization behavior under non-isothermal and isothermal crystallization conditions was investigated. The results showed that this glass exposed complex primary crystallization. In the temperature range < 800 °C primary phase is $K_{3.8}Nb_5Ge_3O_{20.4}$, while $K_6Nb_6Ge_4O_{26}$ appeared as primary phase at temperatures > 800 °C. $K_{10}Nb_{22}Ge_4O_{68}$ and metastable KnB_3O_3 and $K_4Nb_6O_{17}$ were formed as secondary phases. The crystallization commenced at $T > 640$ °C with high homogeneous nucleation rate and spherulite crystal growth morphology. DTA curves recorded for powder samples particle size < 0.1 mm revealed three exothermic peaks and three endothermic peaks within temperature range of $T = 640\text{--}940$ °C, while the DTA curves recorded for powder samples particle size > 0.1 mm showed two exothermic peaks and two endothermic peaks within temperature range of $T = 640\text{--}1020$ °C. The analysis of the dominant crystallization mechanism of powder glass sample and kinetics of crystallization is presented.

INTRODUCTION

Glass-ceramics with second-order optical non-linearity are of great scientific and technical interest [1,2]. Nanocrystallization of glasses is an effective method for the fabrication of such materials. It has recently been reported that crystallized glasses in the system of $K_2O\text{--}Nb_2O_5\text{--}GeO_2$ show nanocrystallization [3,4,5]. Transition metal ions with an empty *d* shell, such as Nb^{5+} , contribute to the increase of nonlinear indexes in iono-covalent insulating materials [6]. In the structure of the majority of niobium containing crystal is formed by $[NbO_6]$ octahedra with a different degree of distortion, whereas structures characterized by $[NbO_4]$ tetrahedral are rare since the Nb^{5+} ion is too large to fit into an oxygen-anion tetrahedral [7]. In potassium germanate glass compositions, it was suggested that, the emergence of the octahedral units depends on the GeO_2/K_2O molar ratio and it occurs for Nb_2O_5 contents > 15 mol% [8].

The aim of the present study is a more detailed investigation of the crystallization behavior of potassium niobium germanate glass with ratio $GeO_2/K_2O = 1.2$ and high content of 34 mol% Nb_2O_5 . The investigations were performed under non-isothermal and isothermal crystallization conditions.

EXPERIMENTAL

The glass was prepared by melting a homogeneous mixture of reagent-grade K_2CO_3 , Nb_2O_5 and GeO_2 in a platinum crucible. The melting was performed in an electric furnace BLF 17/3 at $T=1200$ °C during $t=1$ h. The melt was cast and cooled between two steel plates. Powder X-ray diffraction (XRD) analysis confirmed the quenched melts to be vitreous. The samples were transparent, without visible residual gas bubbles.

The chemical composition of the glass was determined using AAS – PERKIN ELMER 300 and JENA SPEKOL 1300 spectrophotometers.

The experiments under non-isothermal conditions were performed using a Netzsch STA 409 EP device and Al_2O_3 powder as the reference material. Powder samples of the following granulations were prepared: $<0.037\text{--}0.048$; $0.048\text{--}0.063$; $0.063\text{--}0.1$; $0.1\text{--}0.2$; $0.2\text{--}0.3$; $0.3\text{--}0.4$; $0.4\text{--}0.5$; $0.5\text{--}0.65$; $0.65\text{--}0.83$ and $0.83\text{--}1.0$ mm. In the experiments, a constant weight (100 mg) of the samples was heated at heating rate $\beta = 10$ °C/min to $T = 1050$ °C. The second group of experiments was performed with granulations <0.037 , which were heated at different rates of 5, 10, 12, 15 and 20 °C/min from 20 °C to $T = 900$ °C.

The experiments with bulk glass samples were performed in a one-stage regime. The samples were heated at heating rate $\beta = 10^\circ\text{C}/\text{min}$ up to the chosen temperature in the range of $T = 630\text{-}900^\circ\text{C}$ at which they were maintained over different periods of time in an electric furnace Carbolite CWF 13/13, with automatic regulation and temperature accuracy of $\pm 1^\circ\text{C}$. Finally, the samples were removed from the furnace and then crushed into an agate mortar. Powdered samples were used for X-ray and fractured ones for SEM analyses.

The XRD method was used to determine the phase composition. The XRD patterns were obtained using a Philips PW-1710 automated diffractometer with a Cu tube operated at 40 kV and 30 mA. The instrument was equipped with a diffracted beam curved graphite monochromator and a Xe-filled proportional counter. The diffraction data were collected in the 2θ Bragg angle range from 5 to 70° , counting for 0.50 s (qualitative identification) and from 10 to 110° for 4 s (quantitative phase analysis-Rietveld method) at every 0.02° step. The divergence and receiving slits were fixed to 1 and 0.1, respectively. All the XRD measurements were performed at room temperature in a stationary sample holder. The LSUCRIPC program was used for the refinement of the cell dimensions from the powder data [9-13]. The quantitative amounts of the crystalline phases in the sample were determined using the full structure matching mode of the Rietveld refinement method [14], using the MAUD program [15].

A Jeol JSM 5800 SC microscope was used for the SEM investigations, and the fractured bulk samples previously sputtered with gold were used.

RESULTS AND DISCUSSION

The results of the chemical analyses of the glass are presented in Table 1. Nominal composition is also given for the purpose of comparison.

As presented in Table 1, the glass composition is close to the nominal with the ratio of $\text{GeO}_2/\text{Nb}_2\text{O}_5 = 1.07$. The structure of this glass can be described as a mixed network formed by GeO_4 tetrahedra and NbO_6 octahedra. The K^+ ions are preferentially located close to the NbO_6 octahedra, thus compensating the excessive negative charges [8].

Figure 1 shows the DTA curves for the samples with particle sizes of <0.048 and $0.5\text{-}0.65$ mm recorded at heating rate $\beta = 10^\circ\text{C}/\text{min}$ in the temperature range of $20\text{-}1050^\circ\text{C}$.

Table 1. Chemical analysis of the glass.

	Oxide, x_i (mol%)		
	K_2O	Nb_2O_5	GeO_2
Nominal	30	34	36
Analyzed	30.22	33.64	36.14

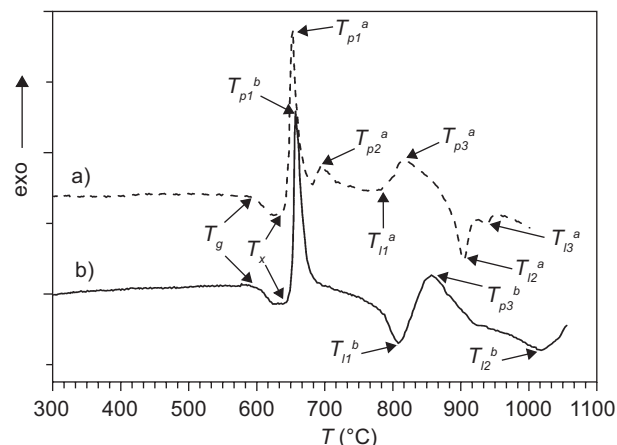


Figure 1. DTA curves recorded at a heating rate of $10^\circ\text{C}/\text{min}$ for powder samples: a) <0.048 and b) $0.5\text{-}0.65$ mm.

The DTA curves showed in Figure 1 are complex. The glass transition temperature, T_g and the first crystallization onset temperature T_x are easily revealed. The difference between the $T_{p1}\text{-}T_g \sim 62^\circ\text{C}$ indicated that this glass is less thermally stable. On the curve a) the noticeable peaks are: (i) three exothermic peaks ($T_{p1}^a, T_{p2}^a, T_{p3}^a$) and (ii) three endothermic peaks ($T_{I1}^a, T_{I2}^a, T_{I3}^a$). On the curve b) the noticeable peaks are: (i) two exothermic peaks (T_{p1}^b, T_{p3}^b) and (ii) two endothermic peaks (T_{I1}^b, T_{I2}^b). All peaks on the curve b) shift toward higher temperatures. These results clearly manifested a significant influence of the particle sizes of powder samples on crystallization behavior of glass. Such behavior also indicates the formation of different crystalline phases during the crystallization. The significant temperatures for the DTA curves recorded (Figure 1) are presented in Table 2.

Table 2. The significant temperatures on DTA curves recorded at heating rate of $10^\circ\text{C}/\text{min}$ for powder samples of particle size a) < 0.048 and b) $0.5\text{-}0.65$ mm.

DTA curve	(°C)							
	T_g	T_x	T_{p1}	T_{p2}	T_{p3}	T_{I1}	T_{I2}	T_{I3}
a	591	639	654	695	816	782	904	937
b	595	643	657	—	856	808	1018	—

The experiments on bulk samples under isothermal conditions were performed in order to identify the formed crystal phases. In one-step regime, the samples were heated at $T = 630\text{-}900^\circ\text{C}$ for different periods of time. Figure 2 shows the XRD patterns of the glass samples crystallized at different temperatures.

Figure 2 demonstrates that several crystalline phases appeared, which clearly indicates a complex primary crystallization of this glass. The phase present in the largest amount crystallizes as the primary one. The others appear as secondary phases. According to the results of XRD, the crystallization of this glass commences by formation

of three crystalline phases: $K_{3.8}Nb_5Ge_3O_{20.4}$ as primary and $K_4Nb_6O_{17}$ and $K_6Nb_6Ge_4O_{26}$ as secondary ones (Figure 2b - peak 1 on the DTA curves from Figure 1). At temperature of crystallization $T = 700^\circ\text{C}$ (Figure 2c), the $K_{3.8}Nb_5Ge_3O_{20.4}$ is also present as primary phase, and $K_6Nb_6Ge_4O_{26}$, $K_4Nb_6O_{17}$ and $KNbO_3$ as secondary ones. At this temperature, the content of $K_4Nb_6O_{17}$ is smaller than at $T = 650^\circ\text{C}$, while the content of $K_6Nb_6Ge_4O_{26}$ is increased. As a new secondary phase, the $KNbO_3$ appeared. On the DTA curve (Figure 1a), in the vicinity of this temperature one smallest peak 2 is observed, which could be related to the appearance of the new $KNbO_3$ phase. However, the peak 2 appeared only on the DTA curves recorded for the samples particle size $< 0.1 \text{ mm}$. On the DTA curves recorded for the samples particle size $> 0.1 \text{ mm}$, the peak 2 does not appear. This indicates that the new phase $KNbO_3$ was formed rapidly by the surface crystallization mechanism, whereby its contribution to the whole DTA signal influenced the appearance of peak 2. By increasing the glass particle size, the contribution of formation of this phase to the whole DTA signal decreases and the peak 2 is not visible. At crystallization temperature $T = 800^\circ\text{C}$ (Figure 2d), $K_6Nb_6Ge_4O_{26}$ is present as the primary phase, and $K_{3.8}Nb_5Ge_3O_{20.4}$ and

$KNbO_3$ as the secondary ones. The phase $K_4Nb_6O_{17}$ did not appear. On both DTA curves (Figure 1a and 1b), in the vicinity of this temperature, one endothermal peak T_{l1} appeared which is more visible on the curve b. It can be concluded that this peak represents melting of the $K_4Nb_6O_{17}$ phase. At crystallization temperature $T = 860^\circ\text{C}$ (Figure 2e), the primary phase is $K_6Nb_6Ge_4O_{26}$, and the present secondary ones are: $K_{3.8}Nb_5Ge_3O_{20.4}$, $K_{10}Nb_{22}Ge_4O_{68}$ and $KNbO_3$. $K_{10}Nb_{22}Ge_4O_{68}$ appeared as a new secondary phase. On the DTA curves (Figure 1a and 1b), in the vicinity of this temperature the appearance of the exothermal peak 3 was noted that could be related to the formation of a new $K_{10}Nb_{22}Ge_4O_{68}$ phase. At crystallization temperature $T = 900^\circ\text{C}$ (Figure 2f), $K_6Nb_6Ge_4O_{26}$ is the primary phase too, and $K_{3.8}Nb_5Ge_3O_{20.4}$ and $K_{10}Nb_{22}Ge_4O_{68}$ as secondary ones are present. At this temperature the phase $KNbO_3$ is not present. On the DTA curves (Figure 1a and 1b), above this temperature one endothermal peak T_{l2} is visible, and it may be concluded that this peak shows melting of the $KNbO_3$ phase.

The quantitative fractions of the crystalline phases were determined at the sample annealed at $T_c = 800^\circ\text{C}$ for $t_c = 200 \text{ h}$. The XRD pattern of this sample was recorded in the 2θ range $10-110^\circ$, with a step of 0.02°

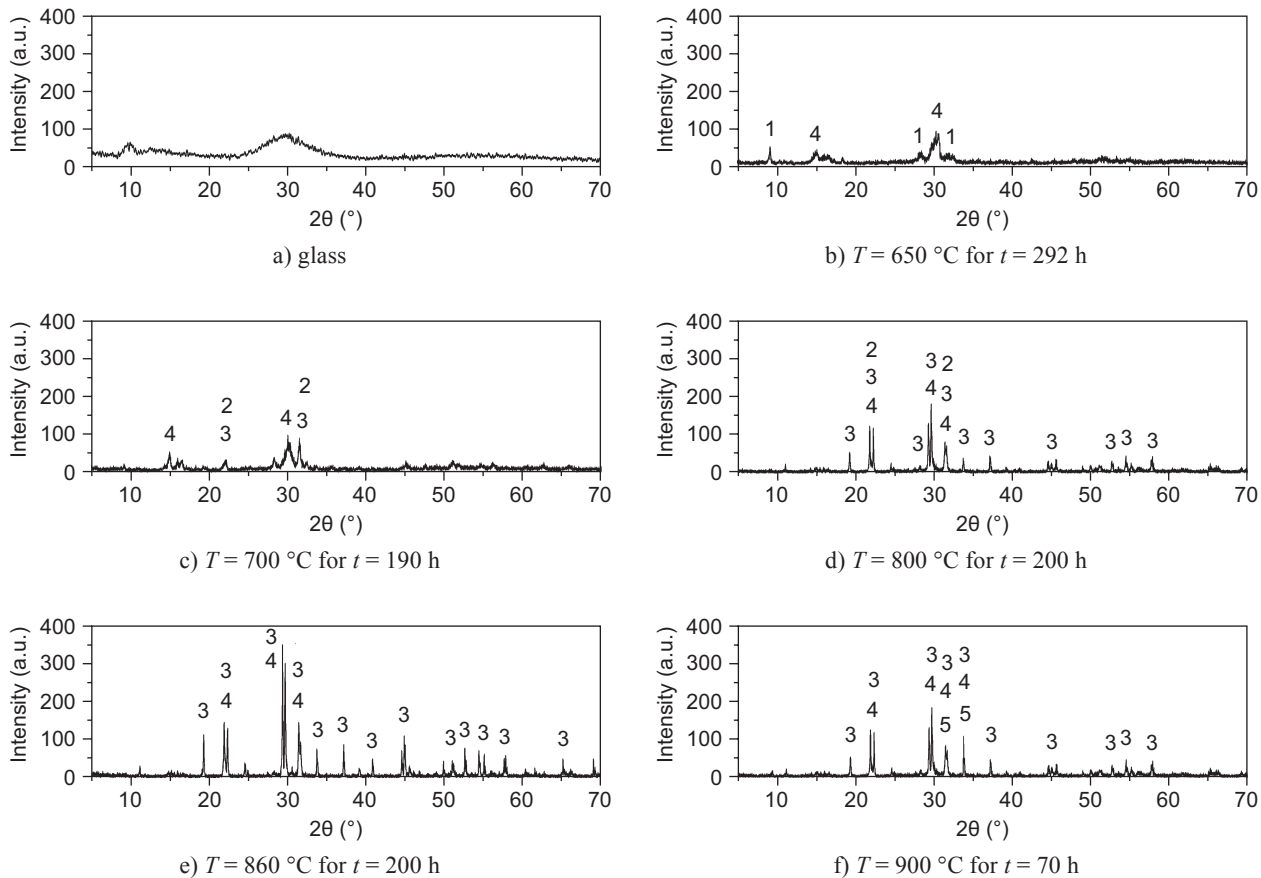


Figure 2. 3D XRD patterns of: a) glass and glass samples annealed at b) $T = 650^\circ\text{C}$ for $t = 292 \text{ h}$, c) $T = 700^\circ\text{C}$ for $t = 190 \text{ h}$, d) $T = 800^\circ\text{C}$ for $t = 200 \text{ h}$, e) $T = 860^\circ\text{C}$ for $t = 200 \text{ h}$ and f) $T = 900^\circ\text{C}$ for $t = 70 \text{ h}$. Peaks marked: 1 - $K_4Nb_6O_{17}$ - JCPDS 53-0780 [9], 2 - $KNbO_3$ - JCPDS 71-2171 [10], 3 - $K_6Nb_6Ge_4O_{26}$ - JCPDS 83-2086 [11], 4 - $K_{3.8}Nb_5Ge_3O_{20.4}$ - JCPDS 77-0963 [12] and 5 - $K_{10}Nb_{22}Ge_4O_{68}$ - JCPDS [13].

and a time of 4 s. A Rietveld profile matching mode fitting plot of this sample is presented in Figure 3, while the results of the fitting are shown in Table 3. The results show that this undercooled melt crystallized into a three component glass-ceramic, with $K_6Nb_6Ge_4O_{26}$ as the primary phase, and $K_{3.8}Nb_5Ge_3O_{20.4}$ and $KNbO_3$ as the secondary ones. The calculated unit cell dimensions were compared to the literature data and no divergence of any kind was registered [14,15]. Table 3 demonstrates that the crystals of all three phases are nanosize, while the smallest ones are those of $K_{3.8}Nb_5Ge_3O_{20.4}$ (52.1 nm).

The undercooled melts generally crystallize by either surface or volume mechanism. Although these crystallization mechanisms can occur simultaneously and competitively, one mechanism usually dominates. The one of the procedure convenient for evaluating the dominant crystallization mechanism of glass powder is Differential thermal analysis (DTA) [16]. Experimental and theoretical studies have shown that the particle size of glass powder influences the mechanism of its crystallization [17-19]. The parameters of $T_p^2/(\Delta T)_p$ and $(dT)_p$ show the dependency on particle size and can be used as qualitative measures by polymorphic and primary surface and volume crystallization. The ratio $T_p^2/(\Delta T)_p$, where T_p is the DTA peak temperature and $(\Delta T)_p$ is the half-width of the DTA peak, is related to the dimension of crystal growth and the height of the exothermal DTA

peak $(dT)_p$ is proportional to total number of nuclei (volume and surface) contained in the glass particle. If surface and volume crystallization proceed simultaneously, three distinct regions can be distinguished as a function of particle size. They reflect the behavior arising from decreasing of surface-to-volume ratio with the increase of particle size.

To determine the dominant crystallization mechanism of this glass, DTA curves of glass powder samples of particle sizes 0-1 mm were recorded at a heating rate of $\beta = 10^\circ\text{C}/\text{min}$.

The effects of particle size on the exothermal DTA peak temperatures, T_p , are presented in Figure 4. It demonstrates that both T_{p1} and T_{p3} increase with the increase of particle size of glass sample. Such behavior also indicates an increase in the resistance to crystallization of this glass.

The results of the influence of particle size on the ratio $T_p^2/(\Delta T)_p$ and DTA peak height $(dT)_p$ for peak 1 and 3 are shown in Figure 5. As observed from Figure 5a for peak 1, complex curves with three distinguishable regions were obtained. For average particle size < 0.050 mm, the ratio $T_p^2/(\Delta T)_p$ and the DTA exothermal peak height $(dT)_p$ decrease with the increase of particle size. The behavior of these parameters is in accordance with theoretical predictions for the case of the predominant surface mechanism of crystallization [18]. In that case

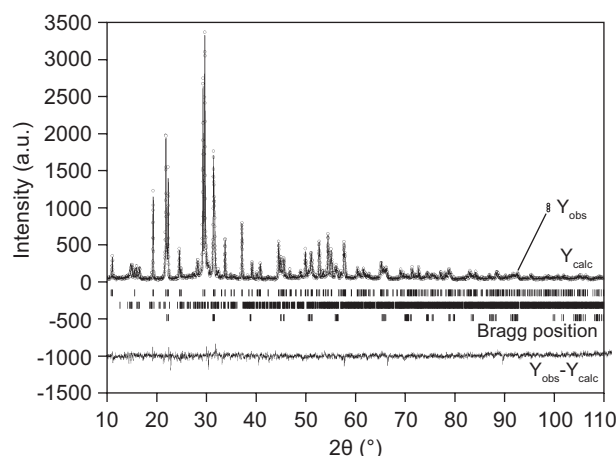


Figure 3. Rietveld refinement plot of the glass sample annealed at: $T = 800^\circ\text{C}$ for $t = 200$ h.

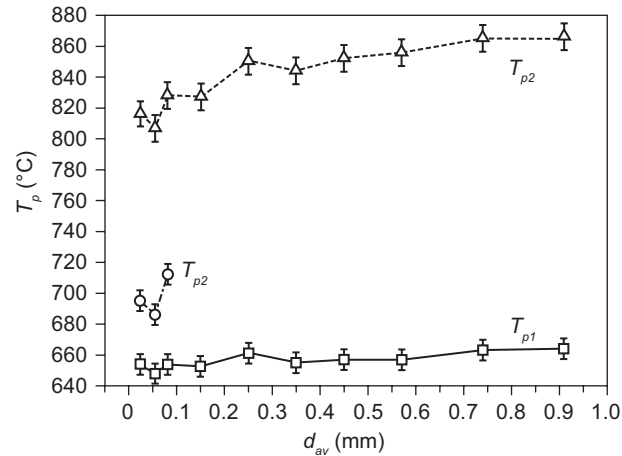


Figure 4. The effect of particle sizes on the exothermal DTA peak temperatures.

Table 3. The most important crystallographic parameters for crystalline phases, obtained from Rietveld refinement of XRD pattern.

Reliability factors (%)			Unit cell parameters			Quantitative fraction (%)		Microstructure	
Rwp	Rb	Rp	a (Å)	b (Å)	c (Å)	Vol.	Wt.	Size (Å)	Microstrain
14.66	11.15	9.71							
Phase									
$K_6Nb_6Ge_4O_{26}$			9.190(2)	9.190(2)	8.132(2)	64.63	64.40	7586	2.01×10^{-4}
$K_{3.8}Nb_5(Ge_5O_9)O_{11.4}$	7.005(2)		12.387(4)	22.113(6)		23.07	22.04	521	6.40×10^{-4}
$KNbO_3$			3.9772(6)	5.686(1)	5.709(1)	12.29	13.56	1306	5.26×10^{-4}

the surface nuclei dominate in the total number of nuclei. The ratio of particle surface to volume decreases with the increase of particle size, as does the number of surface nuclei, i.e., the total number of nuclei. It occurs in case of this glass and only in a narrow particle size interval (smallest particle size). In the range of 0.05–0.15 mm, both curves display minima. In that case the number of surface nuclei is reduced to such an extent that it is equalized with the number of volume nuclei and the total number of the present nuclei is the smallest. In the range of 0.15–0.35 mm both parameters increase to asymptotic values. The ratio of volume to surface in this case grows with the increase of particle sizes too, i.e. the number of volume nuclei increases related to the number of surface nuclei. In the size range >0.35 mm both parameters remain approximately constant. In this sizes range the number of volume nuclei dominates in the total number of nuclei, so that the volume crystallization mechanism prevails. When the number of volume nuclei becomes dominant, further increase of particle size does not significantly influence the change in volume nuclei or the total number of nuclei.

Figure 5b shows a change of parameters $T_p^2/(\Delta T)_p$ and $(dT)_p$ with the particle sizes for the DTA peak 3. It demonstrates that curves of similar shape were obtained. However, peak 3 is significantly smaller in height and width, and according to that the determination of the parameters $T_p^2/(\Delta T)_p$ and $(dT)_p$ are less reliable. In the temperature range of peak 3, the sample is already crystallized. The formation of new phase on peak 3 occurs by transformation of the existing phases, the ones present in the whole volume of the sample. The curves in Figure 5b show that both parameters $T_p^2/(\Delta T)_p$ and $(dT)_p$ increase with the increase of particle size up to 0.35 mm, and then for particle size >0.35 mm both parameters remain approximately constant. These results lead to conclusion that in the temperature range of peak 3 in the particle size range of <0.35 mm the surface and volume crystallization proceed simultaneously. Volume

crystallization mechanism prevails in case of particle size >0.35 mm. The surface crystallization mechanism is not dominant on the DTA peak 3.

The experiments with bulk samples under isothermal conditions were performed (Table 4) in order to check this behavior.

Table 4. Heat treatments condition.

T_c (°C)	t_c (h)
630	1; 3; 5; 360
650	1; 2; 2.5; 3; 5; 24; 292
700	190
800	200
860	200
900	70

The samples annealed for long periods of time were used for XRD analysis (Figures 2 and 3). At the temperatures of crystallization $T_c > 650^\circ\text{C}$, the samples become opaque after short periods of thermal treatment, so that it was impossible to define the crystallization mechanism (surface or volume). The samples annealed for shorter periods of time at $T = 630$ and 650°C were used for analysis of crystallization mechanism and determination of nucleation rate. The SEM micrographs of the interior surface of sample thermally treated in one-stage regime at $T = 630$ and 650°C are shown in Figure 6.

SEM micrograph in Figure 6a shows the spherical-shaped crystals measuring from 20 to 100 nm in diameter. The density of crystals increased with the increase of temperature and the duration of thermal treatment (Figure 6b). In Figure 6c the microstructure of the interior surface of the sample thermally treated at $T = 800^\circ\text{C}$ for $t = 200$ h is shown. The XRD pattern of this sample is presented in Figure 2d, showing that $\text{K}_6\text{Nb}_6\text{Ge}_4\text{O}_{26}$ as primary phase and $\text{K}_{3.8}\text{Nb}_5\text{Ge}_3\text{O}_{20.4}$ and

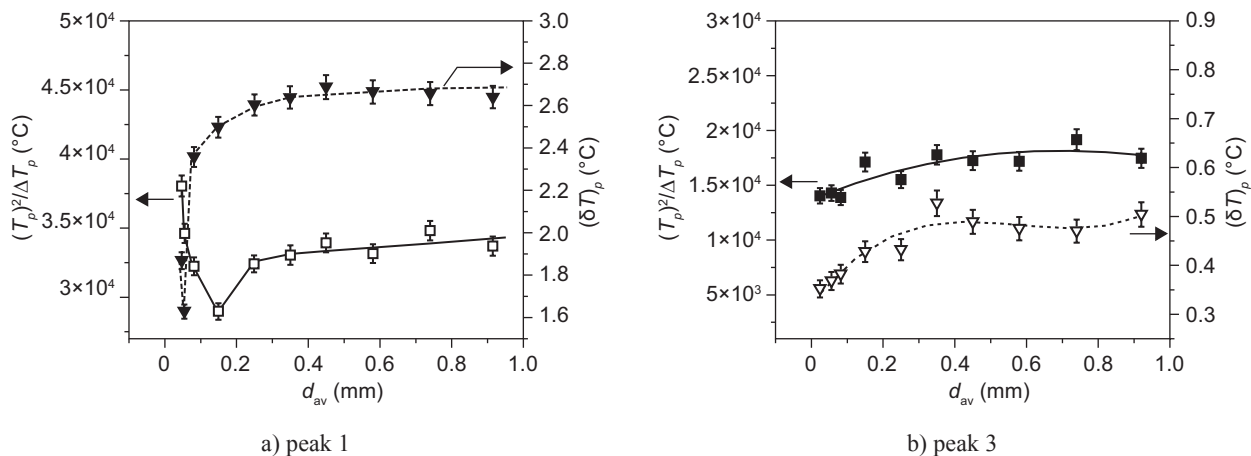


Figure 5. Effect of particle size on the ratio $T_p^2/(\Delta T)_p$ and the DTA exothermal peak height $(\delta T)_p$.

KNbO_3 as secondary ones. These results indicate that these phases in glass are formed by volume crystallization mechanism with spherulite crystal growth morphology.

The results of SEM investigation were used for analysis of nucleation rate in this glass at $T=650\text{ }^\circ\text{C}$. The

number of particles per unit area, N_A , and the diameters of the circular intersections of the particles were determined from the SEM micrographs. The number of particles per unit volume, N_V , was determined from the ratio of N_A and the largest circular cross-section diameter, d , [20]. The nucleation rate, $I = 1.77 \times 10^{14} \text{ m}^{-3} \text{ s}^{-1}$, at the treatment temperature, $T = 650\text{ }^\circ\text{C}$, was determined from the time dependence of the number of particles (spherulites) per unit volume, N_V , (Figure 7). The results showing that the number of particles per unit area, N_A , can be measured directly after a single-stage heat treatment at $T = 650\text{ }^\circ\text{C}$, and indicate that the crystal growth rates in the temperature interval of nucleation have considerable values. Consequently, the temperature interval of nucleation and crystal growth overlapped. This was indicated by vicinity of the temperatures T_g and T_{p1} on DTA curves, Figure 1.

The above presented results suggest that the crystallization process of this glass is very complex. For this reasons, the analysis of the crystallization kinetics is not simple. Non-isothermal methods are convenient, require small sample masses and are relatively easy to perform. However, the majority of the non-isothermal methods has been criticized for assuming an Arrhenian temperature dependence of the transformation kinetics and hence do not have general validity [21,22]. The temperature dependence of the nucleation rate, I , is far from Arrhenian, and the temperature dependence of the crystal growth rate, U , is also not Arrhenian when a broad range of temperatures is considered. This makes the calculated kinetic parameters reliable in certain controlled cases [23]. Within a sufficiently limited temperature range (such as the range of crystallization peaks in DTA), both I and U can be described by the approximations:

$$I = I_0 \times \exp(-E_N/RT) \quad (1)$$

and

$$U = U_0 \times \exp(-E_G/RT) \quad (2)$$

where E_N and E_G are the effective activation energies for nucleation and crystal growth, respectively. In case of isothermal crystallization with I and U independent of time, t , the volume fraction crystallized, x , is obtained by the Kolmogorov-Avrami equation [24-26]:

$$x = 1 - \exp[-(Kt)^n] \quad (3)$$

where n is the Avrami exponent, which is a dimensionless constant related to the nucleation and growth mechanisms. The K is defined as the reaction rate constant, which is usually assigned an Arrhenian temperature dependence:

$$K = K_0 \times \exp(-E/RT) \quad (4)$$

where E is the effective activation energy describing the overall crystallization process. In Eq. (3) $K^n \approx I \times U^m$, where m denotes the dimensionality of crystal growth. Hence, the assumption of an Arrhenian temperature

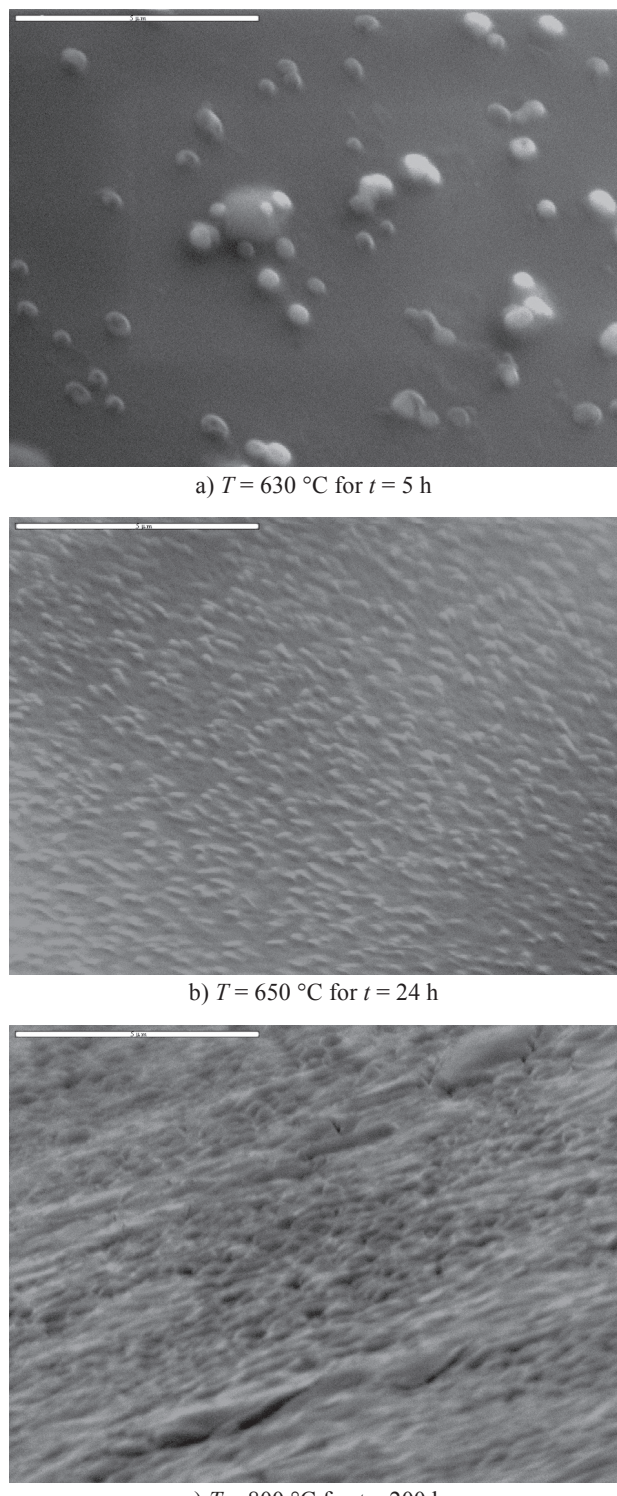


Figure 6. SEM micrographs of glass samples annealed at: a) $T = 630\text{ }^\circ\text{C}$ for $t = 5\text{ h}$, b) $T = 650\text{ }^\circ\text{C}$ for $t = 24\text{ h}$, c) $T = 800\text{ }^\circ\text{C}$ for $t = 200\text{ h}$.

dependence for K is appropriate when I and U vary in an Arrhenian manner with T . From Equations (1) - (4), the overall effective activation energy for crystallization is expressed as [27]:

$$E \approx (E_N + m E_G)/n \quad (5)$$

This assumption holds under following conditions: The nucleation rate is negligible, *i.e.* the condition of site saturation. The occurrence of site saturation in crystal nucleation enables the complicated temperature dependence of the nucleation rate to be neglected and if the temperature dependence of the crystal growth rate is dominated by that of the viscosity, the reaction rate coefficient, K , can reasonably be approximated as Arrhenian over a temperature range around the temperature of the crystallization peak. This condition allows the crystallization process to be considered as an isokinetic reaction, *i.e.* the crystallization rate is dependent only on temperature and not on the previous thermal history.

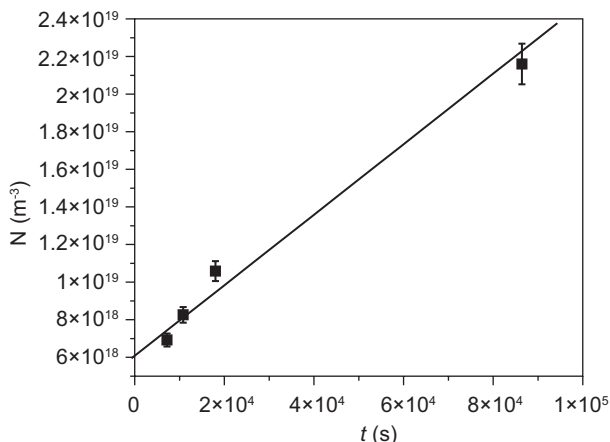


Figure 7. The number of particles per unit volume, N_v , as a function of time at the heat treatment temperature $T = 650^\circ\text{C}$.

The previous results showed that in the range of the smallest granulation, of the total number of nuclei present, the number of surface nuclei was dominant with respect to the internal ones. Therefore the number of nuclei does not significantly change with heating, while the crystal growth rate becomes considerable. Moreover, the results of SEM investigations under isothermal conditions indicated spherulite crystal growth morphology. Such a morphology is associated with continuous growth by the screw dislocation mechanism and interface controlled kinetics of crystal growth. For this case Matusita and Saka [28,29] derived the equation for the analysis of non-isothermal crystallization as:

$$\ln \frac{\beta^n}{T_p^2} = - \frac{m \cdot E_a}{R \cdot T_p} + \text{const.} \quad (6)$$

where R is the gas constant. The values of parameters n and m depend on the rate controlling mechanism of the

crystallization kinetics, while the value of E_a is obtained from the ratio $\ln(\beta^n/T_p^2)$ vs. $1/T_p$ using the corresponding values for n and m . Accordingly, to satisfy the condition of the constant number of nuclei during crystal growth, the glass powder with smallest particle size of < 0.037 mm was chosen. Since the crystal growth in these DTA experiments occurred on a constant number of nuclei, $n = m = 1$ (surface crystallization) and Equation (6) becomes the same as the well-known Kissinger equation [30]. For the analysis of the crystallization kinetics, the T_{pl} temperatures recorded for the powder samples of particle size < 0.037 mm at different heating rates are presented in Table 5. Using the temperatures T_{pl} , the activation energy of crystal growth of $E_a = 499 \pm 66$ kJ/mol was calculated by applying the Kissinger equation.

Table 5. Temperature of the crystallization peak, T_{pl} , for different heating rates β of powder samples of particle size < 0.037 mm.

Particle size	T_{pl} ($^\circ\text{C}$)	β ($^\circ\text{C}/\text{min}$)				
		5	10	12	15	20
< 0.037	644	653	654	655	657	

In this case Ozawa method [31] can also be applied using the relationship:

$$\ln(\beta) = -(E_{a,oz} / R T_p) + \text{const.} \quad (7)$$

Equation (7) calculates the activation energy of crystal growth $E_{a,oz} = 510 \pm 68$ kJ/mol. These results show good agreement between the activation energies of crystal growth determined under non-isothermal condition at peak 1.

CONCLUSIONS

The crystallization behavior of potassium niobium germanate glass composition of $30\text{K}_2\text{O}\cdot34\text{Nb}_2\text{O}_5\cdot36\text{GeO}_2$ (mol%) was studied. Investigations were performed under non-isothermal and isothermal conditions using DTA, XRD and SEM methods. The results showed the primary crystallization of this glass, and a very complex crystallization process was evidenced. The germanium containing phases were formed as primary stable phases, while the phases without germanium were formed as secondary metastable phases. The crystallization process took place with high homogeneous nucleation rate and spherulite crystal growth morphology. Nanostructured samples were obtained.

Analysis of the dominant crystallization mechanism of the powder glass sample showed that the behaviors of the parameters $T_p^2/(\Delta T)_p$ and $(dT)_p$ depend only on the change in the surface-to-volume nuclei ratio, as is the case with polymorphic crystallization. At crystallization peak in temperature range $T < 700^\circ\text{C}$, the

surface crystallization is dominant in the particle size range <0.15 mm. In the range of 0.15-0.35 mm the mixed crystallization mechanism is dominant and the volume crystallization in the range > 0.35 mm. At crystallization peak in temperature range $T > 800$ °C in the particle size range < 0.35 mm the mixed crystallization mechanism is dominant and the volume crystallization in the range >0.35 mm. The surface crystallization mechanism is not dominant in this temperature range.

The kinetics of crystallization was examined by DTA under non-isothermal conditions with powder samples of particle sizes < 0.037 mm at different heating rates. The surface crystallization was detected in the sample with particle sizes < 0.037 mm. The crystallization peaks T_p increased with the increase of heating rate. At crystallization peak in temperature range $T < 700$ °C, the crystal growth occurred on a constant number of nuclei and the activation energy of crystal growth was calculated as $E_a = 499 \pm 66$ kJ/mol.

Acknowledgment

The authors are grateful to the Ministry of Education and Science, Republic of the Serbia for financial support (Projects 172004 and 34001).

References

1. Pernice P., Aronne A., Sigaev V.N., Sarkisov P.D., Molev V.I., Stefanovich S.Yu.: *J.Am.Ceram.Soc.* **82**, 3447 (1999).
2. Sigaev V.N., Stefanovich S.Y., Champagnon B., Gregora I., Pernice P., Aronne A., LeParc R., Sarkisov P.D., Dewhurst C.: *J. Non-Cryst.Solids* **306**, 238 (2002).
3. Narita K., Takahashi Y., Benino Y., Fujiwara T., Komatsu T.: *Opt. Mater.* **25**, 393 (2004).
4. Benino Y., Takahashi Y., Fujiwara T., Komatsu T.: *J. Non-Cryst.Solids* **345&346**, 422 (2004).
5. Narita K., Takahashi Y., Benino Y., Fujiwara T., Komatsu T.: *J. Am. Ceram. Soc.* **87**, 113 (2004).
6. Lines M.E.: *Phys.Rev. B* **43**, 11978 (1991).
7. Jehng J.M., Wachs I.E.: *Chem. Mater.* **3**, 100 (1991).
8. Kolobkova E.V.: *Soviet. J. Glas. Phys.Chem.* **13**, 176 (1988).
9. Powder Diffraction File, Card No. 53-0780. Joint Committee on Powder Diffraction Standards (JCPDS), Swarthmore, PA.
10. Powder Diffraction File, Card No. 71-2171. Joint Committee on Powder Diffraction Standards (JCPDS), Swarthmore, PA.
11. Powder Diffraction File, Card No. 83-2086. Joint Committee on Powder Diffraction Standards (JCPDS), Swarthmore, PA.
12. Powder Diffraction File, Card No. 77-0963. Joint Committee on Powder Diffraction Standards (JCPDS), Swarthmore, PA.
13. Powder Diffraction File, Card No. 83-1500. Joint Committee on Powder Diffraction Standards (JCPDS), Swarthmore, PA.
14. Rietveld H.M.: *J. Appl. Cryst.* **2**, 65 (1969).
15. L. Lutterotti, (2009), MAUD version 2.074, <http://www.ing.unitn.it/~maud/>.
16. Ray C.S., Yang Q., Haung W., Day D.E.: *J. Am. Ceram. Soc.* **79**, 3155 (1996).
17. Ray C.S., Day D.E., Haung W., Lakshmi Narayan K., Cull T.C., Kelton K.F.: *J. Non-Cryst. Solids* **204**, 1 (1996).
18. Kelton K.F., Lakshmi Narayan K., Levine L.E., Cull T.C., Ray C.S.: *J. Non-Cryst. Solids* **204**, 13 (1996).
19. Tošić M.B., Živanović V.D., Grujić S.R., Stojanović J.N., Nikolić J.D.: *J. Non-Cryst. Solids* **354**, 3694 (2008).
20. Gonzales Oliver C.J.R., Russo D.O., James P.J.: *Phys. Chem. Glasses* **45**, 100 (2004).
21. Yinnon H., Uhlmann D.R.: *J. Non-Cryst. Solids* **54**, 253 (1983).
22. Weiberg M.C.: *J. Non-Cryst. Solids* **127**, 151 (1991).
23. Šesták J.: *Phys. Chem. Glass* **15**, 137 (1974).
24. Kolmogorov A.: *Izv. Acad. Sci. USSR, Ser.Math.* **1**, 355 (1937).
25. Avrami M.: *J. Chem. Phys.* **7**, 1103 (1939).
26. Avrami M.: *J. Chem. Phys.* **8**, 212 (1940).
27. Šesták J.: *Phys. Chem. Glass* **15**, 137 (1974).
28. Matusita K., Sakka S.: *Phys. Chem. Glasses* **20**, 81 (1979).
29. Matusita K., Sakka S.: *J. Non-Cryst. Solids* **34**, 741 (1980).
30. Kissinger H.E.: *Anal. Chem.* **29**, 1072 (1959).
31. Ozawa T.: *J. Thermal Analysis* **9**, 369 (1976).